


## Research Article

# Mathematical Physics Modelling and Prediction of Oil Spill Trajectory for a Catenary Anchor Leg Mooring (CALM) System

Xuanze Ju <sup>1,2</sup>, Zili Li,<sup>1</sup> Baohui Dong,<sup>2</sup> Xianwu Meng,<sup>2</sup> and Shuguang Huang<sup>2</sup>

<sup>1</sup>College of Pipeline and Civil Engineering, China University of Petroleum (East China)/Shandong Key Laboratory of Oil & Gas Storage and Transportation Safety, Qingdao 266580, China

<sup>2</sup>Offshore Oil Engineering Co., Ltd., Engineering Company, Tianjin 300451, China

Correspondence should be addressed to Xuanze Ju; [juxz@cnooc.com.cn](mailto:juxz@cnooc.com.cn)

Received 15 April 2022; Revised 11 May 2022; Accepted 19 May 2022; Published 3 June 2022

Academic Editor: Meraj Ali Khan

Copyright © 2022 Xuanze Ju et al. This is an open access article distributed under the Creative Commons Attribution License, which permits unrestricted use, distribution, and reproduction in any medium, provided the original work is properly cited.

The catenary anchor leg mooring (CALM) system usually moored a heavy oil tanker; due to its complex working mechanism and special working environment, oil spill accidents are easy to happen. Once the oil spill accident happens, it not only causes huge economic loss, but also kills the marine ecological environment. Oil spill trajectory model considers almost all weathering processes including evaporation, emulsification, dispersion, dissolution, photooxidation, sedimentation, and biodegradation. Model simulations indicated that both tidal currents and wind drag force have significant effect in oil spill movement. The dominant wind in the area is South-westerly wind during the summer monsoon and North-easterly wind during the winter monsoon, but South-westerly wind is far stronger and last longer than the North-easterly wind. As a result, oil spill trajectory is most likely towards offshore to North-east during the summer period (April to September). During the winter period (November–January), oil spill would move towards shore under North-westerly winds. Once oil reaches shore, it would stay at shore permanently and eventually sink to seabed or beach in the simulation. Although the model does not consider longshore drift by waves, oil movement along shore by waves would be a slow process. Therefore, the impact of oil spill during the winter monsoon would be limited to local area around Ras Markaz.

## 1. Introduction

The transport of petroleum products to export destinations is conducted either by pipeline or in oil terminals. Onshore and offshore terminals are the common types of oil terminals. However, due to geographical and economic conditions, the number of ports available for the construction of oil terminals is limited, resulting in the increase of secondary transport costs, the detention of oil tankers arriving at a port, and other issues. Therefore, it is necessary to study other types of offshore oil loading/offloading facilities to cooperate with or replace oil terminals. The most common type of offshore terminal is the single point mooring (SPM) of catenary anchor leg mooring (CALM) type. A typical schematic for the CALM system is shown in Figure 1 [1]. Since the CALM

system was introduced in 1958 [2], it has operated 85% of the world's 700 oil terminals [3, 4], with extensive operations in Southeast Asia, the Middle East, and West Africa. In particular, deepwater offloading CALM buoys are being extensively used in West Africa to allow the efficient loading of spread-moored FPSO [5], and the maximum applied water depth has reached 1435 meters (Agbami oil field, Nigeria) [6]. But for the CALM system, due to its complex working mechanism and special working environment, oil spill accidents are easy to happen [7]. Once the oil spill accident happens, it not only causes huge economic loss, but also kills the Marine ecological environment.

Oil spills have been occurring at sea with increasing frequency, pose significant threats to the marine environment, and often lead to devastating effects on local marine ecology

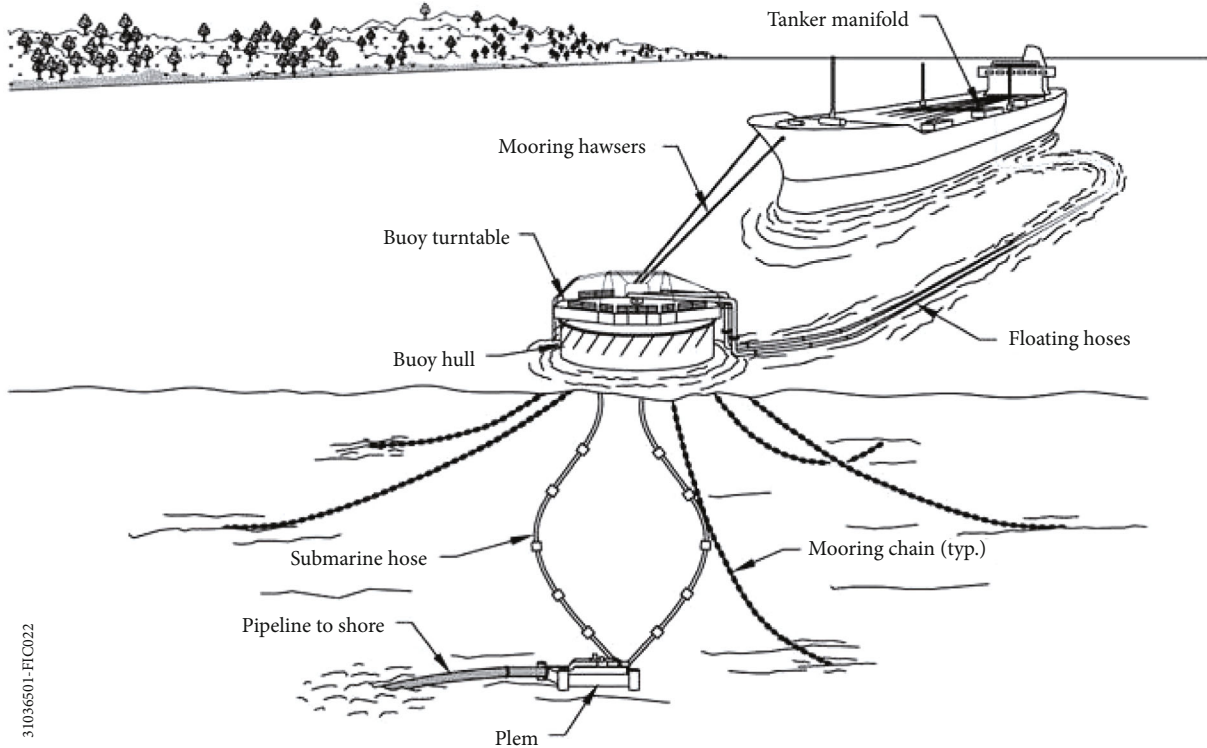


FIGURE 1: Schematic of a typical catenary anchor leg mooring (CALM) system.

[8]. Numerical modeling has become an important tool for oil spill forecasting, which allows for real time effective clean-up operations immediately after the occurrence of oil spill accidents. Thus, recent years have seen a rapid development of various mathematical models for simulating and predicting oil spills. However, the movement and variation of oil spill in the sea is a complex process, which is influenced by physical, chemical, and biological processes, and is related to the marine hydrodynamic conditions, meteorological conditions, and the oil properties. The processes include oil film expansion, drift, evaporation, emulsification, dissolution, sedimentation, and adsorption. The study on oil spills began in the 1960s. Up to now, many scholars in the world have established and perfected lots of oil spill models. These may include advection, turbulent diffusion, evaporation, dissolution, emulsification, dispersion, auto-oxidation, biodegradation, and sinking/sedimentation [9]. In the last five and six decades, many researchers have studied the processes of oil spills, and various oil spill models have been proposed [10]. Fay [11] divided the oil film expansion into three stages: inertial expansion, viscous expansion, and surface tension expansion, but did not consider the influence of wind on horizontal diffusion. Lehr [12] considered the influence of wind and established a modified Fay-type spreading equation. Elliott [13] proposed the oil particle method for the first time, which regards the oil spill as a large number of oil particles and does not need to solve the diffusion equation. More and more oil spill models begin to use the Lagrange oil particle algorithm, which has become the mainstream method of oil spill trajectory prediction.

Chao et al. [14] established two-dimensional and three-dimensional oil spill models in Singapore coastal waters using an oil particle algorithm. Wang et al. [15] established a double-layer oil particle model. Sebastião and Guedes Soares [16] introduced a method to determine the uncertainties in the predictions of oil spill trajectories using a classic oil spill model. The method considers the output of the oil spill model as a function of random variables, which are the input parameters, and calculates the standard deviation of the output results which provides a measure of the uncertainty of the model as a result of the uncertainties of the input parameters. Vethamony et al. [17] presented an oil spill occurred off Goa, west coast of India, on 23 March 2005 due to collision of two vessels. The MIKE21 Spill Analysis model was used to simulate the spill trajectory. The observed spill trajectory and the slick area were in agreement with the model simulations. Díaz et al. [18] used the probabilistic particle tracking model to simulate the oil diffusion after the oil spill from the Prestige wreck in Galicia. Guo and Wang [19] based on an oil particle algorithm, combined with the 3-D free-surface hydrodynamics model and the third-generation wave model, simulated the oil release in Dalian coastal waters. Mariano et al. [20] developed two oil particle trajectory prediction systems and applied them to the 2010 Deepwater Horizon oil spill in the Gulf of Mexico. Yu et al. [21] proposed a random walk parameterization hindcast method (RWPHM) for the Bohai Sea, in which random walk is initially parameterized and combined with remote sensing data and oil-spill models. Perianez [22] established a Lagrangian oil spill transport model for the

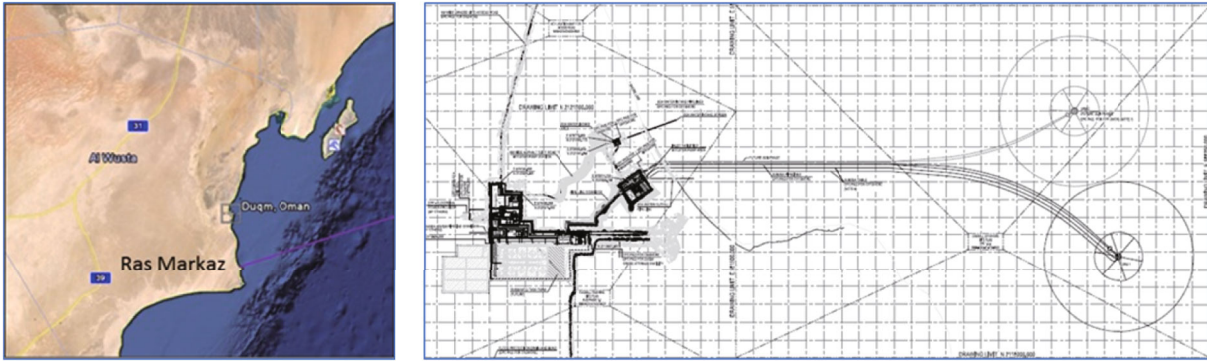


FIGURE 2: Location of Ras Markaz Crude Oil Park.

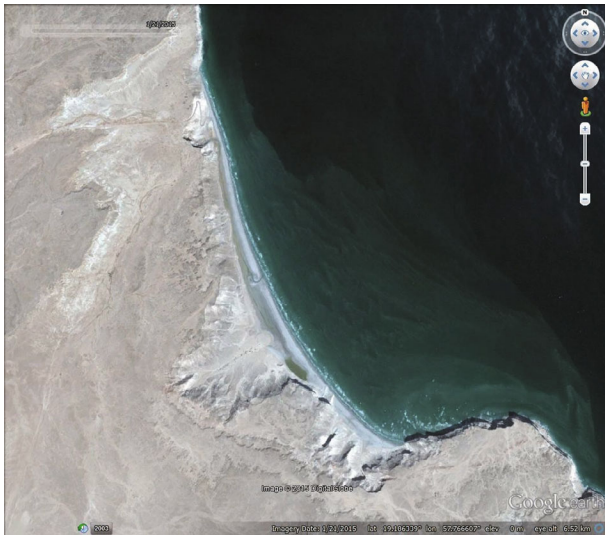


FIGURE 3: Plan shape of Ras Markaz crenulated bay.



FIGURE 4: View of the crenulated bay from the northern headland (Ras Markaz is in the background).

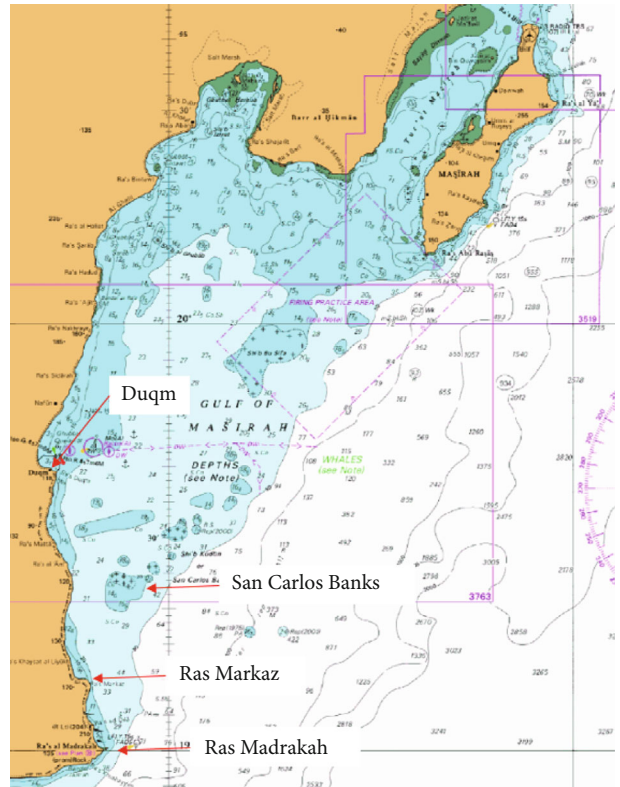


FIGURE 5: Gulf of Masirah.

Red Sea. The weathering process includes evaporation, emulsification, natural dispersion, dissolution, photooxidation, sedimentation, adhesion to materials, interaction with mineral fines, biodegradation, and the formation of tarballs

[23]. Mohamed et al. [24] presented the oil is introduced to the marine environment; it undergoes a series of natural processes known as “weathering.” For a successful response operations and protection, it is critical to precisely estimate the behavior of the spilled oil. Debra and William [25] adapted the Fractions Skill Score method, commonly used in weather forecasting, to oil forecasting. A subset of satellite images and trajectory forecasts from the Deepwater Horizon oil spill are used as an example of the method. Pan et al. [26] demonstrated an operational oil spill forecasting system established by National Marine Environmental Forecasting Center (NMEFC). Satellite observations, oil spill models, and operational met-oceanographic forecasts are integrated into the system. Until now, many researchers have



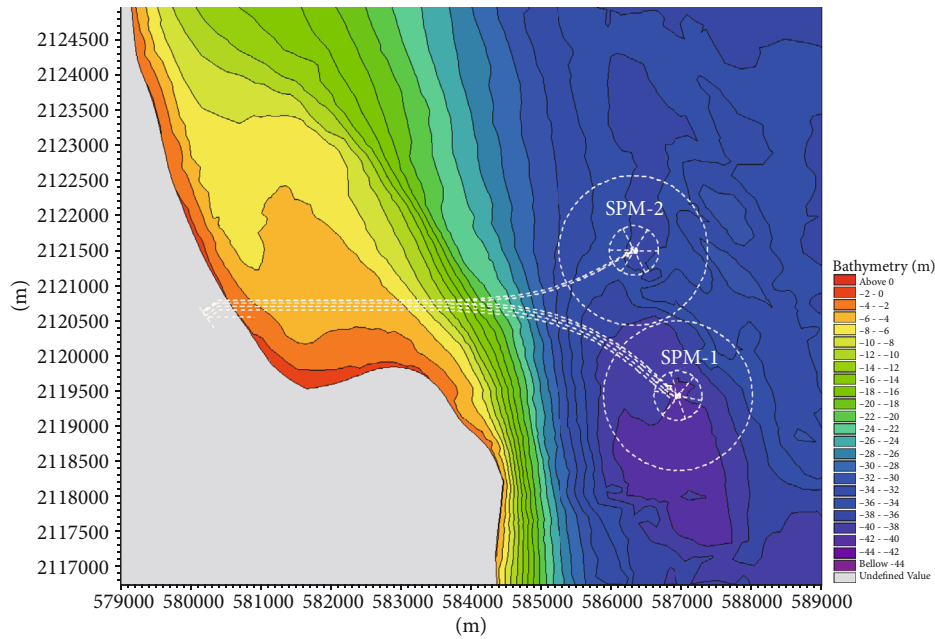


FIGURE 6: Nearshore bathymetry of Ras Markaz crenulated bay.

investigated the weathering process of the oil spill [27–29], in which empirical formula based on laboratory test is the most commonly used method to calculate oil spill weathering [30]. At present, some of the most widely used oil spill models that can predict the process of oil spill transportation and fate are as follows: Oil Spill Risk Analysis (OSRA), OILTRANS, Oil Modeling Application Package (OILMAP), General National Oceanic and Atmospheric Administration Operational Oil Modeling Environment (GNOME), Oil Spill Contingency and Response (OSCAR), MEDSLIK-II, Estuarine Oil Spill Model (EOSM), and MIKE21 SA model [31–37].

This study presents the oil spill trajectory modelling completed for the planning and design of the Crude Oil Storage Terminal at Ras Markaz on the eastern Arabian Sea coast. The location of the site and layout of the marine facilities, which include two SPMs of CALM type and associated pipelines, are shown in Figure 2. The purpose of the modelling is to investigate the trajectory and fate of potential oil spills through dispersion under the action of the tides, currents, and winds.

## 2. Site Conditions

**2.1. Geological and Geomorphological Setting.** The Ras Markaz site is located at the southern end of a large shallow bay extending from Ras Madrasah in the south to Masirah Island in the north. There is a northerly movement of sediment through this large bay driven by wave conditions in the monsoon season. This results in the accretion of sediment at the northern extremity of the bay to the west of Masirah Island and within the channel between the island and the mainland. At Ras Markaz, the oil pipeline trench is located at the southern end of a shallow crenulated bay cre-

ated by differential erosion between Ras Markaz headland in the south and a less prominent headland in the north (Figure 3). The headland cliffs are composed of layered carbonate rocks (Figure 4).

**2.2. Bathymetry and Locations of Oil Pipelines & SPMs of CALM Type.** The large bay extending from Ras Madrasah up to Masirah Island has a wide and shallow bathymetry with depths generally less than 30 m. This bathymetry is illustrated in Figure 5. The nearshore bathymetry of the smaller bay at Ras Markaz can be broken down into three zones (Figure 6). At the Ras Markaz headland, the bathymetry is steep with the 10 m contour approximately 500 m from the coastline. For most of the crenulated bay, the nearshore gradients are significantly shallower with the 10 m contour that is approximately 2.5 km from the coast. In the southern half of the bay, the nearshore contains a shallow “plateau” at around 3–6 m water depth with steeper slopes inland and seaward of it. This might indicate a significant build-up of sand in these areas, forming a wide nearshore bar. It is likely that sediment transported north has migrated around Ras Markaz headland and into the crenulated bay where the sand bar has formed. There may also be a contribution of sediment from the local Wadi. In the north of the Ras Markaz bay, there is a shallow area, San Carlos Banks (see Figure 5). This shallow water has been identified as a potential risk area of vessel grounding and has been selected for this oil spill trajectory modelling. The oil pipelines and SPM are located to the south of the bay (Figure 6).

### 2.3. Physical Processes

**2.3.1. Wind Climate.** The wind climate along the coast between Ras Madrasah and Masirah Island is dominated

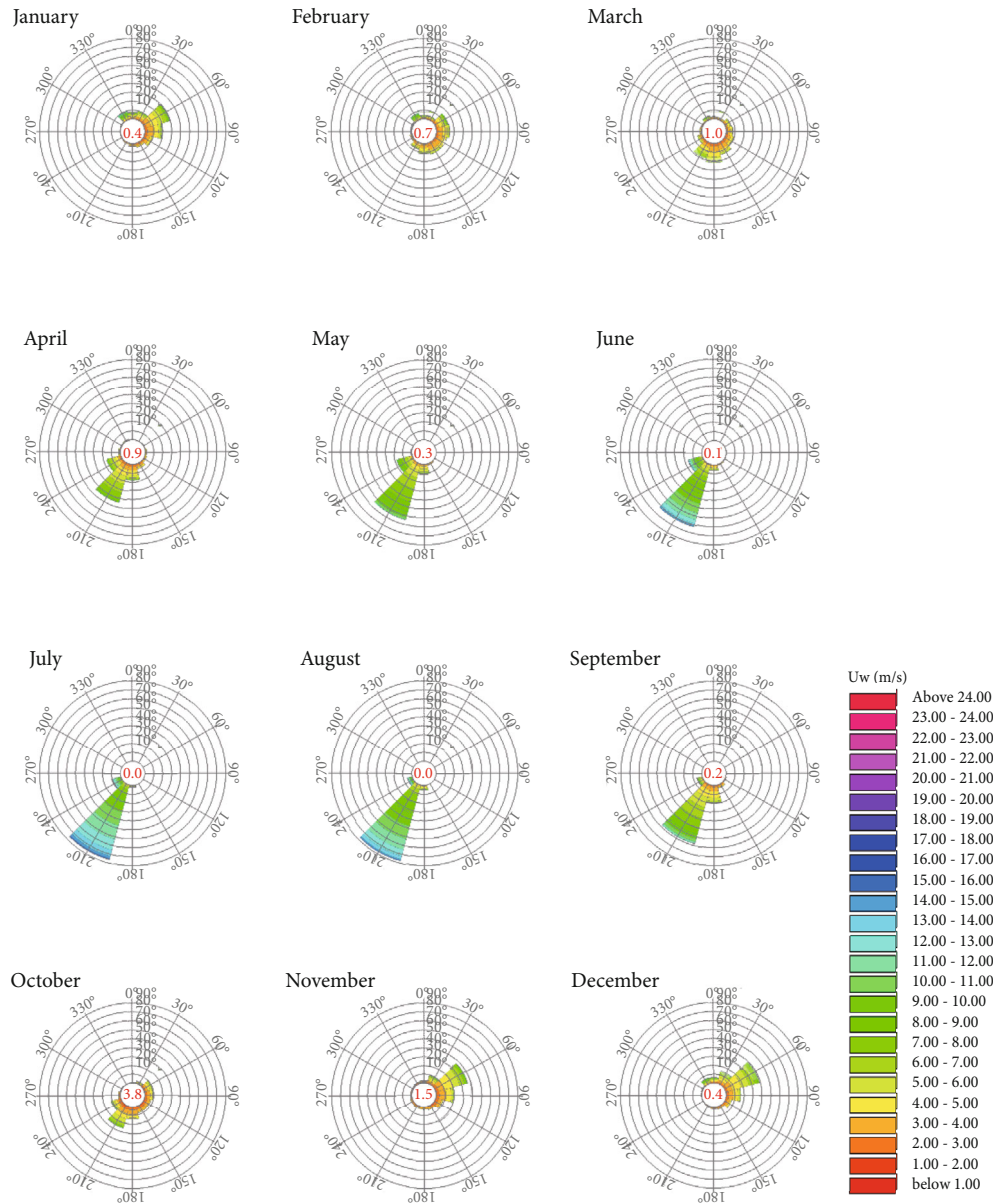


FIGURE 7: Wind roses (hindcasted wind data from Oceanweather).

TABLE 1: Wind frequency (hindcasted wind data from Oceanweather).

Wind speed (m/s)	0°N	30°N	60°N	90°N	120°N	150°N	180°N	210°N	240°N	270°N	300°N	330°N	Total
0–3	0.57%	0.74%	1.20%	1.52%	1.64%	1.63%	1.62%	1.40%	0.89%	0.48%	0.40%	0.41%	12.5%
3–5	0.71%	1.41%	5.05%	4.90%	3.06%	2.96%	5.17%	4.83%	1.68%	0.42%	0.35%	0.52%	31.1%
5–7	0.64%	1.07%	4.06%	1.29%	0.39%	0.57%	2.84%	8.77%	2.07%	0.15%	0.13%	0.67%	22.7%
7–9	0.31%	0.49%	1.22%	0.12%	0.02%	0.03%	0.48%	9.70%	1.66%	0.01%	0.02%	0.68%	14.7%
9–11	0.09%	0.09%	0.15%	0.01%	0.00%	0.01%	0.03%	8.30%	1.13%	0.00%	0.01%	0.48%	10.3%
11–13	0.01%	0.01%	0.02%	0.00%	0.00%	0.00%	0.00%	5.56%	0.72%	0.00%	0.00%	0.12%	6.5%
13–15	0.01%	0.01%	0.00%	0.00%	0.00%	0.00%	0.00%	1.92%	0.32%	0.00%	0.00%	0.01%	2.3%
Total	2.45%	3.8%	11.7%	7.8%	5.1%	5.2%	10.1%	40.5%	8.5%	1.2%	0.9%	2.9%	100%

by the two monsoon seasons. In the summer monsoon (April–September), the prevailing conditions are from south-west. Outside this season, the wave climate is more

moderate with prevailing winds from the north-east. Figure 7 illustrates monthly and annual wind roses in off-shore based on hindcasted wind data provided by

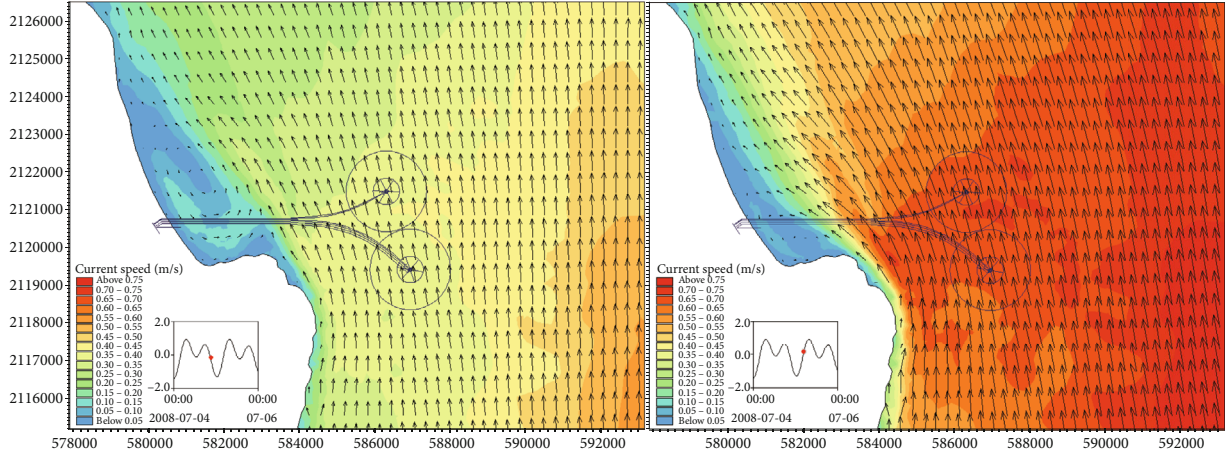


FIGURE 8: Depth-averaged current velocity during spring tide of the summer monsoon (left: ebb and right: flood tides).

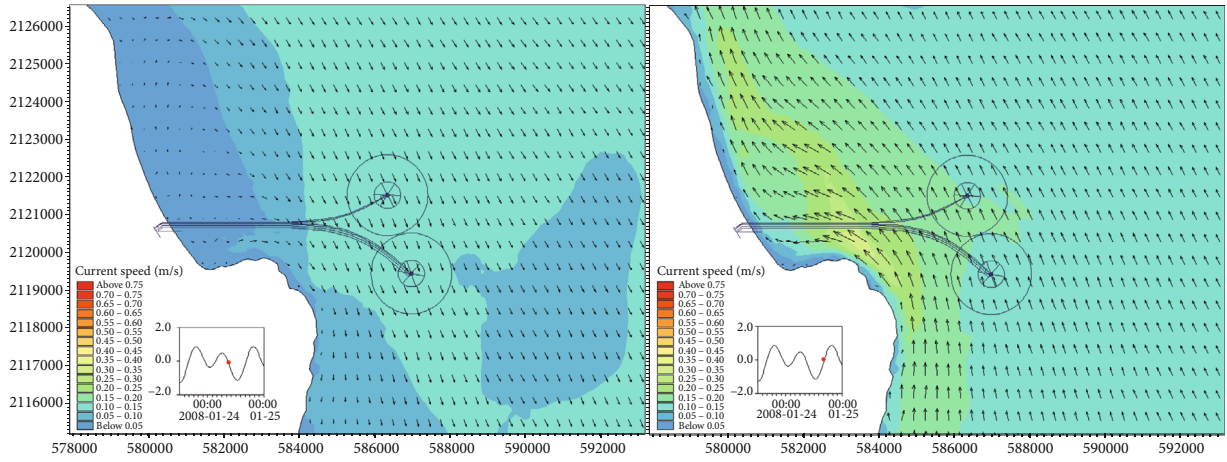


FIGURE 9: Depth-averaged current velocity during spring tide of the winter monsoon (left: ebb and right: flood tides).

Oceanweather. Table 1 presents the offshore wind data in wind frequency.

**2.3.2. Tidal Range.** Local tides are mixed semi-diurnal. The range at the Ras Markaz site is approximately 1.5m (between mean higher high water and mean lower low water) with highest and lowest astronomical tide at +2.54 m CD and +0.14 m CD, respectively.

**2.3.3. Tidal Currents.** Currents at the site are broadly aligned with the coastline. Flows in a north/north-westerly direction dominate during the summer monsoon season. Outside this season, flows are generally in south easterly direction. Currents are stronger during the monsoon season with flows up to 0.5 m/sec at SPM1. The 1 in 1 year current at this location is 1 m/sec driven by strong winds associated with the storm event.

Figures 8 and 9 illustrate modelled peak ebb and flood tidal currents in the area during the summer and winter monsoons, respectively. They show that tidal current velocities (depth-averaged) close to shore are low (less than

0.05 m/s to 0.35 m/s locally) increasing further offshore (greater than 0.5 m/s).

### 3. Methodology

#### 3.1. Governing Equations of Tidal Current Motion

##### 3.1.1. Continuity Equation.

$$\frac{\partial \zeta}{\partial t} + \frac{\partial[(h + \zeta)u]}{\partial x} + \frac{\partial[(h + \zeta)v]}{\partial y} = 0. \quad (1)$$

##### 3.1.2. Momentum Equation.

$$\begin{aligned} \frac{\partial u}{\partial t} + u \frac{\partial u}{\partial x} + v \frac{\partial u}{\partial y} - fv \\ = -g \frac{\partial \zeta}{\partial x} + \frac{\partial}{\partial x} \left( N_x \frac{\partial u}{\partial x} \right) + \frac{\partial}{\partial y} \left( N_y \frac{\partial u}{\partial y} \right) - f_b \frac{\sqrt{u^2 + v^2}}{h + \zeta} u, \end{aligned}$$

$$\begin{aligned} & \frac{\partial v}{\partial t} + u \frac{\partial v}{\partial x} + v \frac{\partial v}{\partial y} + fu \\ & = -g \frac{\partial \zeta}{\partial y} + \frac{\partial}{\partial x} \left( N_x \frac{\partial v}{\partial x} \right) + \frac{\partial}{\partial y} \left( N_y \frac{\partial v}{\partial y} \right) - f_b \frac{\sqrt{u^2 + v^2}}{h + \zeta} v. \end{aligned} \quad (2)$$

where  $\zeta$  is tide level (relative to a datum level);  $T$  is time;  $x$  and  $y$  are cartesian coordinates;  $u$ ,  $v$  is the flow velocity in  $x$  and  $y$  directions;  $h$  is water depth (relative to a datum level);  $N_x$  and  $N_y$  are turbulence viscosity coefficients in  $x$  and  $y$  directions;  $f$  is Coriolis parameter;  $g$  is the acceleration of gravity; and  $f_b$  is the friction coefficient at the bottom.

**3.2. Spatial Discrete Calculation of the Model.** For shallow water equations in the Cartesian coordinate system,  $CFL$  can be defined as

$$CFL_{HD} = \left( \sqrt{gh} + |u| \right) \frac{\Delta t}{\Delta x} + \left( \sqrt{gh} + |v| \right) \frac{\Delta t}{\Delta y}, \quad (3)$$

where  $CFL_{HD}$  is the Courant–Friedrichs–Lewy condition in the hydrodynamic module,  $h$  is the total water depth,  $u$  and  $v$  are the velocity component in  $x$  and  $y$  direction,  $\Delta x$  and  $\Delta y$  are the characteristic distance in  $x$  and  $y$  direction,  $\Delta t$  is the time interval, and  $g$  is the gravitational acceleration.

### 3.3. Oil Spill Trajectory Model

**3.3.1. Expansion Process.** Take the below equation:

$$\frac{dA_o}{dt} = K_a \cdot A_o^{1/3} \cdot \left[ \frac{V_o}{A_o} \right]^{4/3}, \quad (4)$$

where  $A_o$  is the oil film area,  $A_o = \pi R_o^2$ ,  $R_o$  is oil film diameter,  $t$  is time,  $K_a$  is diffusion coefficient;  $V_o = R_o^2 \pi h$ , and  $h$  is the initial oil film thickness.

#### 3.3.2. Transport Process

(i) Drift motion

$$U_t = C_w \cdot U_w + U_s. \quad (5)$$

In  $\Delta t$  time, the position change equation of oil particles is

$$\begin{aligned} X &= X_0 + u \Delta t + C_w U_w \sin \theta \Delta t, \\ Y &= Y_0 + v \Delta t + C_w U_w \cos \theta \Delta t. \end{aligned} \quad (6)$$

where  $X_0$  and  $Y_0$  are the initial position of the oil film;  $U_t$  is the total drift velocity;  $U_s$  is the surface flow velocity;  $u$  and  $v$  are the current velocity;  $U_w$  is the wind speed (10 m above the sea surface);  $\theta$  is the wind direction angle; and  $C_w$  is the wind drift coefficient, usually 0.03-0.04.

(ii) Turbulent diffusion

$$S_a = [R]_{-1}^{+1} \cdot \sqrt{6D_a \Delta t}, \quad (7)$$

where  $S_a$  is the random walking distance in the  $a$  direction within a time step,  $D_a$  is the diffusion coefficient in the  $a$  direction,  $t$  is the diffusion time, and  $[R]_{-1}^{+1}$  is the random number from -1 to 1.

**3.3.3. Weathering Process.** Oil spill model considers almost all weathering processes including evaporation, emulsification, dispersion, dissolution, photooxidation, sedimentation, and biodegradation (see Figure 10).

(i) Evaporation

$$\begin{aligned} \frac{dQ}{dt} &= \frac{K_2 P A_o}{RT} \cdot f \cdot M, \\ K_2 &= k \cdot A_o^{0.045} \cdot S_c^{(-2/3)} \cdot U_w^{0.78}, \end{aligned} \quad (8)$$

where  $dQ/dt$  is the evaporation rate;  $K_2$  is the mass transfer coefficient ( $k$  is the evaporation coefficient,  $S_c$  is the Schmidt number, and  $U_w$  is the wind speed),  $P$  is vapor pressure,  $A_o$  is the oil film area,  $f$  is the evaporation fraction, and  $R$  is the constant

(ii) Emulsification

$$Y_w = \frac{K_A \left( 1 - e^{-K_A K_B (1+U_w)^2 t} \right)}{K_B}, \quad (9)$$

where  $Y_w$  is the moisture content of the emulsion,  $K_A = 4.5 \times 10^{-6}$ ,  $K_B = 1/Y_w$ , and  $Y_w$  is the final moisture content

(iii) Dispersion

$$Q_d = CD^{0.57} SF d^{0.7} \Delta d, \quad (10)$$

where  $C$  is the encoder coefficient,  $D$  is the wave energy dissipation,  $S$  is the fraction of sea surface covered by oil,  $F$  is the fraction covered by broken wave,  $d$  is the average diameter of oil droplets, and  $\Delta d$  is the size interval of oil droplets

(iv) Dissolution

$$\begin{aligned} D_v &= K_1 \cdot A \cdot \frac{M_v}{M_t} \cdot \rho_1 \cdot f_D \cdot C_V, \\ D_h &= K_2 \cdot A \cdot \frac{M_h}{M_t} \cdot \rho_2 \cdot f_D \cdot C_h, \end{aligned} \quad (11)$$



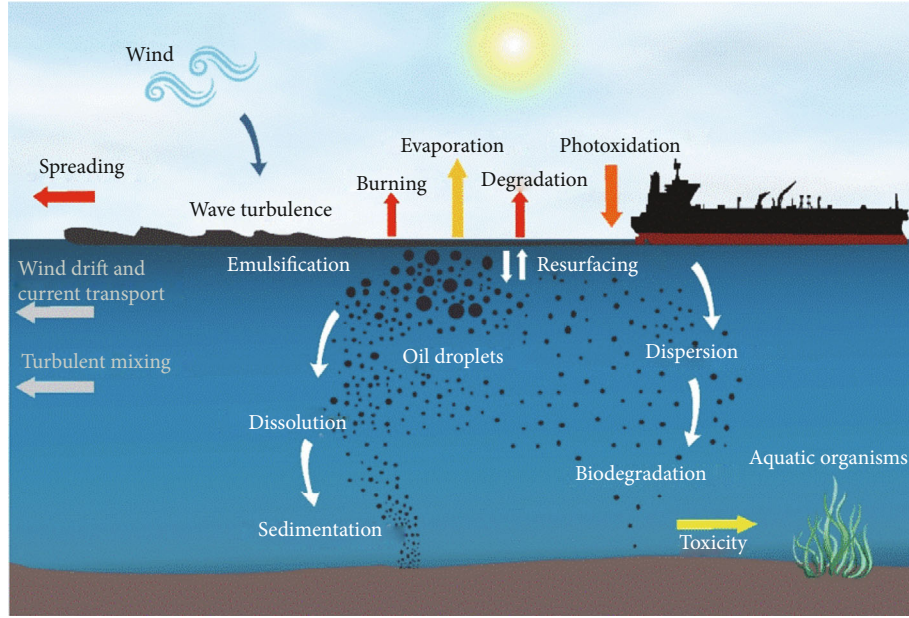


FIGURE 10: Weathering processes of oil in marine environmental in open water.

TABLE 2: Model setup main parameters.

Parameters	Settings
Time step (s)	30
Simulation time after oil release (days)	60
Number of vertical layers	8
Horizontal dispersion coefficients (m <sup>2</sup> /s)	20 in the area around the site where fine mesh is applied; 200 in other areas where coarse mesh is applied
Vertical dispersion coefficients (m <sup>2</sup> /s)	0.01
Number of oil particles release (each run)	720
Oil property	4 fractions of oil (volatile oil, heavy oil, asphaltene and wax) are related to Guafita crude oil
Spreading (terminal thickness) (m)	0.0001
Biodegradation (decay rate in per day)	Volatile fraction: 0.005 Heavy fraction: 0.0 Maximum water fraction: 0.85
Emulsification	Kao constant: 3.3 Kaw constant: 200 Emulsion rate: $2.0 \times 10^{-6}$ s/m <sup>3</sup>
Water solubility (kg/kg)	Volatile fraction: $2.0 \times 10^{-5}$ Heavy fraction: $2.0 \times 10^{-7}$
Volumentric temperature (1/°C)	Volatile fraction: 0.0007 Heavy fraction: 0.0007
Dissolution (per day)	0.4

where  $K_1$  and  $K_2$  are the volatilization and recombination fraction;  $M_v$  and  $M_h$  are the volatilization and recombination fraction mass, respectively;  $M_t$  is the total mass of oil particles;  $\rho_1$  and  $\rho_2$  are the volatilization and recombination fraction density, respectively;  $A$  is the oil film area,  $f_D$  is the chemical dispersant effect; and  $C_v$  and  $C_h$  are the volatilization and recombination fraction water solubility, respectively

### 3.3.4. Heat Transfer Process

- (i) Heat transfer between oil film and air can be expressed as

$$H_T^{\text{oil-air}} = A_{\text{oil}} k_H^{\text{oil-air}} (T_{\text{air}} - T_{\text{oil}}),$$



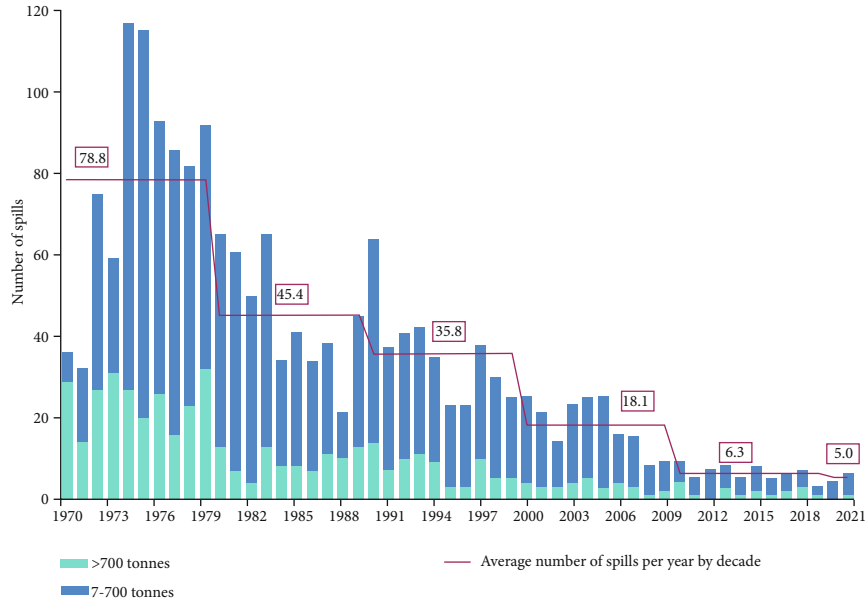


FIGURE 11: Number of oil spills from tankers worldwide, 1970-2021 (ITOPF, 2021).

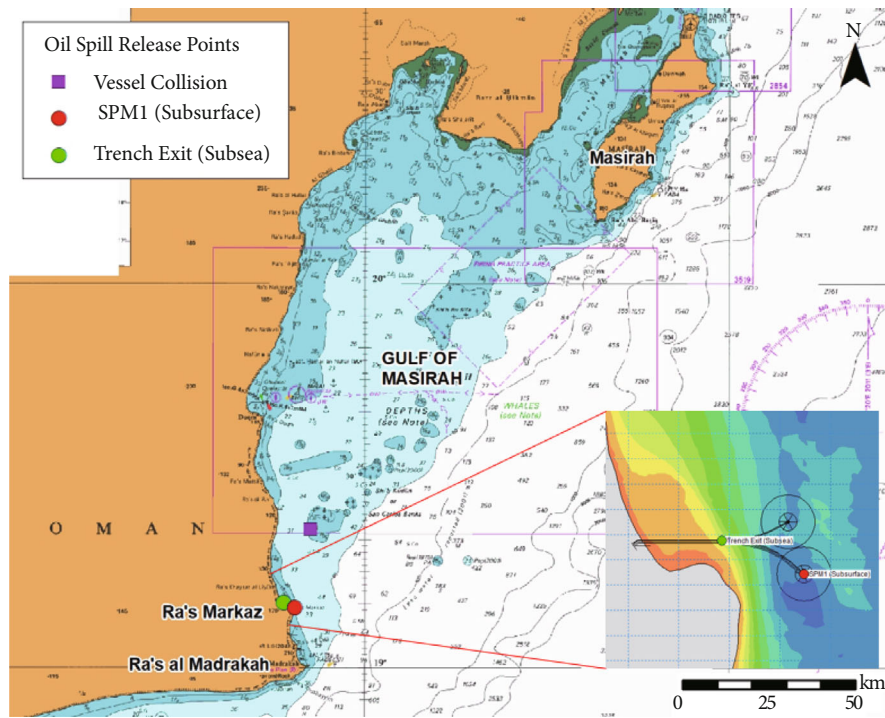


FIGURE 12: Initial oil spill locations.

$$K_H^{\text{oil-air}} = K_m \rho_a C_{pa} \left( \frac{S_c}{P_r} \right)_{\text{air}}^{0.67},$$

$$P_r = \frac{C_{pa} \rho_a}{0.0241(0.18055 + 0.003T_{\text{air}})}, \quad (12)$$

where  $S_c$  is the Schmidt number,  $k_H^{\text{oil-air}}$  is the heat transfer coefficient,  $T_{\text{oil}}$  is the oil film temperature,  $T_{\text{air}}$  is the air temperature,  $P_r$  is the air prandtl

number,  $C_{pa}$  is the atmospheric heat capacity, and  $\rho_a$  is the atmospheric density

(ii) Heat transfer between oil film and water can be expressed as

$$H_T^{\text{oil-water}} = A_{\text{oil}} k_H^{\text{oil-water}} (T_{\text{water}} - T_{\text{oil}}),$$

$$K_H^{\text{oil-water}} = 0.332 + r_w C_{pw} \text{Re}^{-0.5} \text{Pr}_w^{-2/3},$$

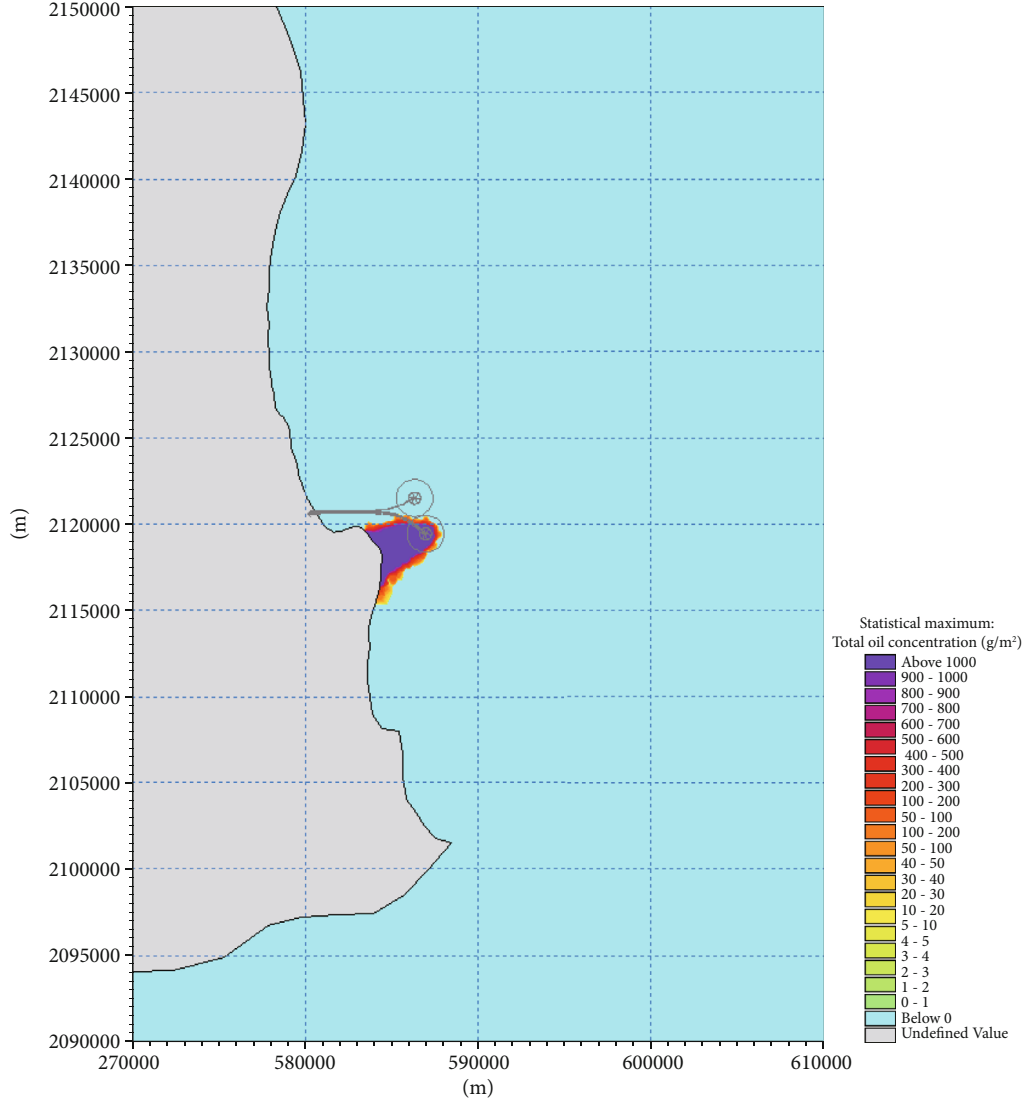


FIGURE 13: Map of maximum oil concentration for scenario 1 (subsurface blowout:  $16,000m^3$  spill at SPM1) (under typical wind in the winter monsoon).

$$Pr_w = C_{pw} V_w \rho_w \left( \frac{1}{0.330 + 0.000848(T_w - 273.15)} \right), \quad (13)$$

where  $T_{water}$  is the temperature of water,  $Pr_w$  is the number of prandtl of water,  $C_{pw}$  is the water heat capacity, and  $\rho_w$  is the density of water

(iii) Solar radiation

$$H(t) = \begin{cases} K_t \cdot H_o^{\max} \cdot \sin \left( \pi \frac{t - t^{\text{sunrise}}}{t^{\text{sunset}} - t^{\text{sunrise}}} \right) & t^{\text{sunrise}} < t < t^{\text{sunset}} \\ 0, & \text{otherwise} \end{cases}, \quad (14)$$

$$t^{\text{sunset}} = t^{\text{sunrise}} + T_d,$$

where  $t^{\text{sunrise}}$  is the sunrise time,  $t^{\text{sunset}}$  is the sunset time, and  $T_d$  is the day length

(iv) Transmitting and receiving radiation

$$H_{\text{total}}^{\text{rad}} = \sigma (l_{\text{air}} \cdot T_{\text{air}}^4 + l_{\text{water}} T_{\text{water}}^4 - 2l_{\text{oil}} T_{\text{oil}}^4), \quad (15)$$

where  $l_{\text{air}}$  is the atmospheric emissivity,  $l_{\text{water}}$  is the water emissivity,  $l_{\text{oil}}$  is the oil emissivity,  $T_{\text{air}}$  is the air temperature,  $T_{\text{water}}$  is the water temperature,  $T_{\text{oil}}$  is the oil temperature, and  $\sigma$  is the Boltzman constant

(v) Evaporative heat loss

$$H^{\text{vapor}} = \sum_i^{\text{numberofcomponents}} N_i \cdot \Delta H_{vi},$$

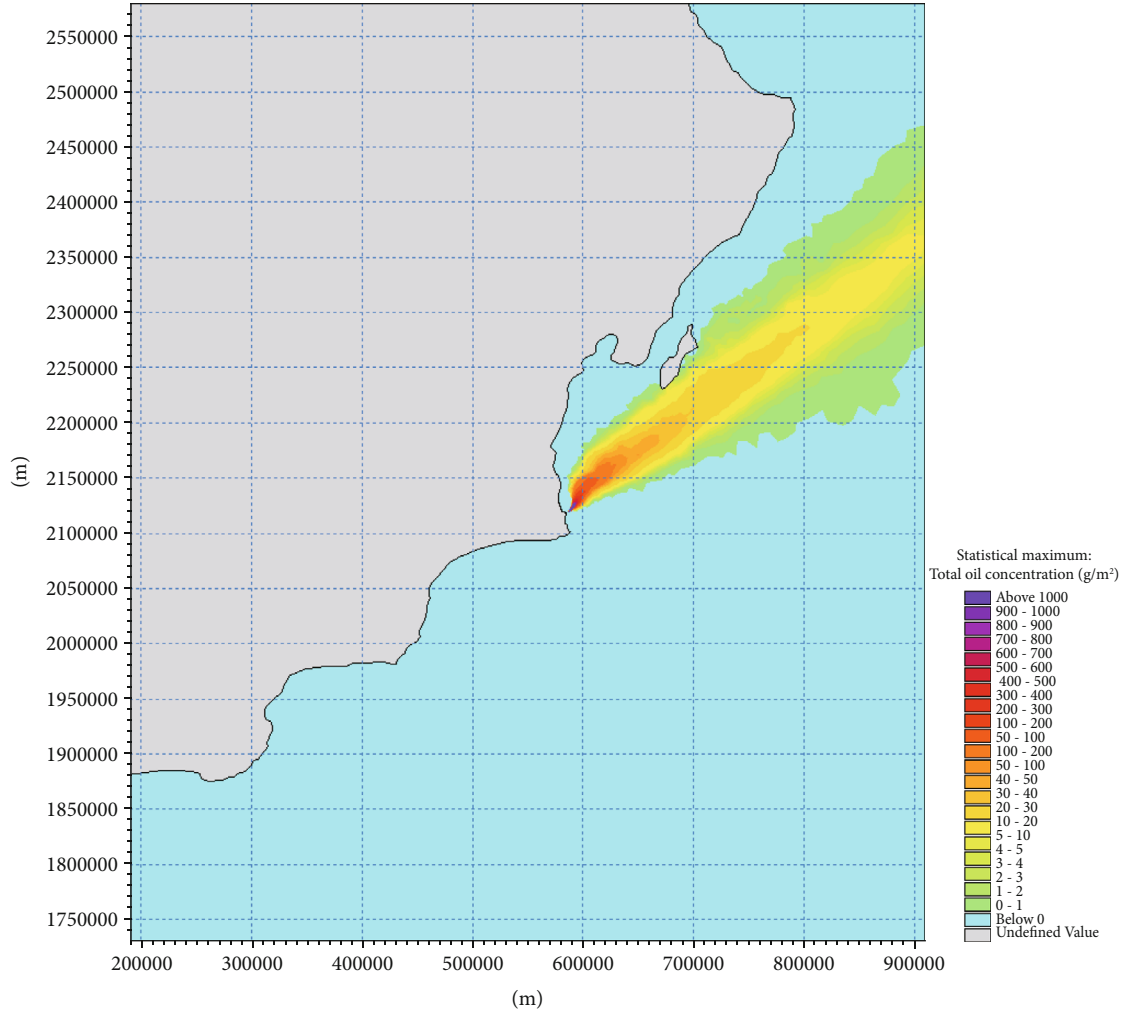


FIGURE 14: Map of maximum oil concentration for scenario 1 (sub-surface blowout:  $16,000m^3$  spill at SPM1) (under typical wind in the summer monsoon).

$$\begin{aligned} \frac{dT_{oil}}{dt} = & \frac{1}{\zeta C_p h} [(1-a)H + (l_{air}T_{air}^4 + l_{water}T_{water}^4 - 2l_{oil} \cdot T_{oil}^4)] \\ & + h_{ow}(T_{water} - T_{oil}) + h_{oa}(T_{air} - T_{oil}) - \sum N_i \Delta H_{vi} \\ & + \left( \frac{dV_{water}}{dt} \zeta_w \cdot C_{pw} + \frac{dV_{oil}}{dt} \zeta_{oil} C_{poil} \right) \\ & \cdot (T_{water} - T_{oil}) \cdot A_{oil}, \end{aligned} \quad (16)$$

where  $\Delta H_{vi}$  is the vaporization heat of  $i$ ,  $dV_{water}/dt$  is the water absorption rate,  $dV_{oil}/dt$  is the amount of oil droplets dispersed by upwelling, and  $C_{po}$  and  $C_{pw}$  are the heat capacity of oil and water, respectively

**3.4. Model Setup.** The model simulation was carried out for a duration of 60 days covering 4 spring-neap tidal cycles for typical summer and winter monsoon wind conditions, and also all-year wind frequency presented in Table 2.

Sensitivity tests have been carried out for an optimized particle number for sensible balance between accuracy and

computational time. The model results have been compared between the use of 720 particles and 7,200 particles, and the difference was found marginal.

**3.5. Modelled Oil Type.** For more accurate predictions of weathering processes, the oil is divided into fractions (so-called pseudo-components). Therefore, for modelling purpose, it is required to find specific oil characteristics, either from a database or by laboratory tests. In this study, approach of describing an oil by 4 fractions, namely, volatile oil, heavy oil, asphaltene and wax, and the established oil spill template. In this oil spill trajectory modelling, Guafita Crude Oil was simulated, which is described by the following 4 fractions [38]:

- (i) Volatile oil: 28.5 (25-32%)
- (ii) Heavy oil: 53% (47-59%)
- (iii) Asphaltene: 16% (10-22%)
- (iv) Wax: 2.5%



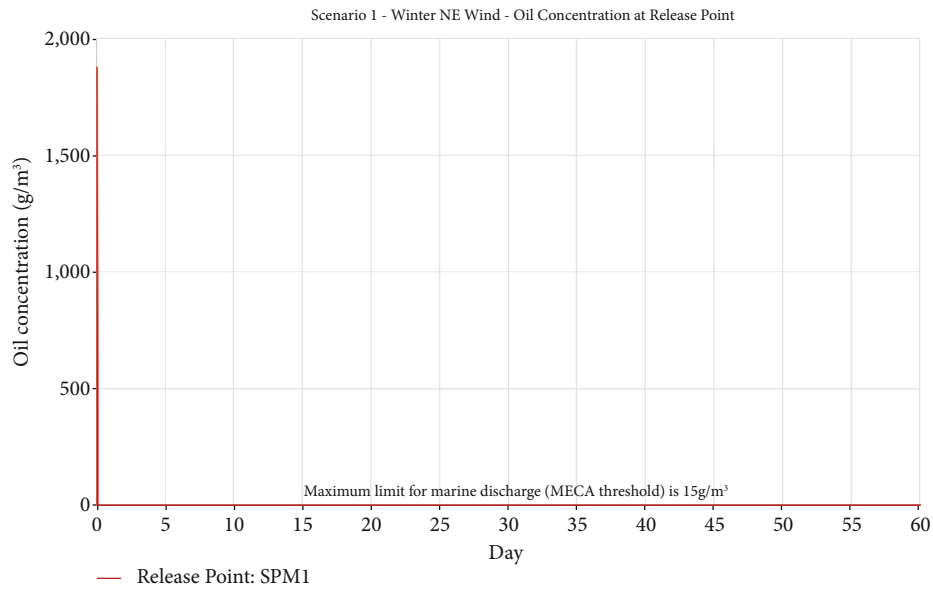


FIGURE 15: Changes in oil concentration over time at SPM1 spill location for scenario 1 (subsurface blowout: 16,000m<sup>3</sup> spill at SPM1) (under typical winter wind condition).

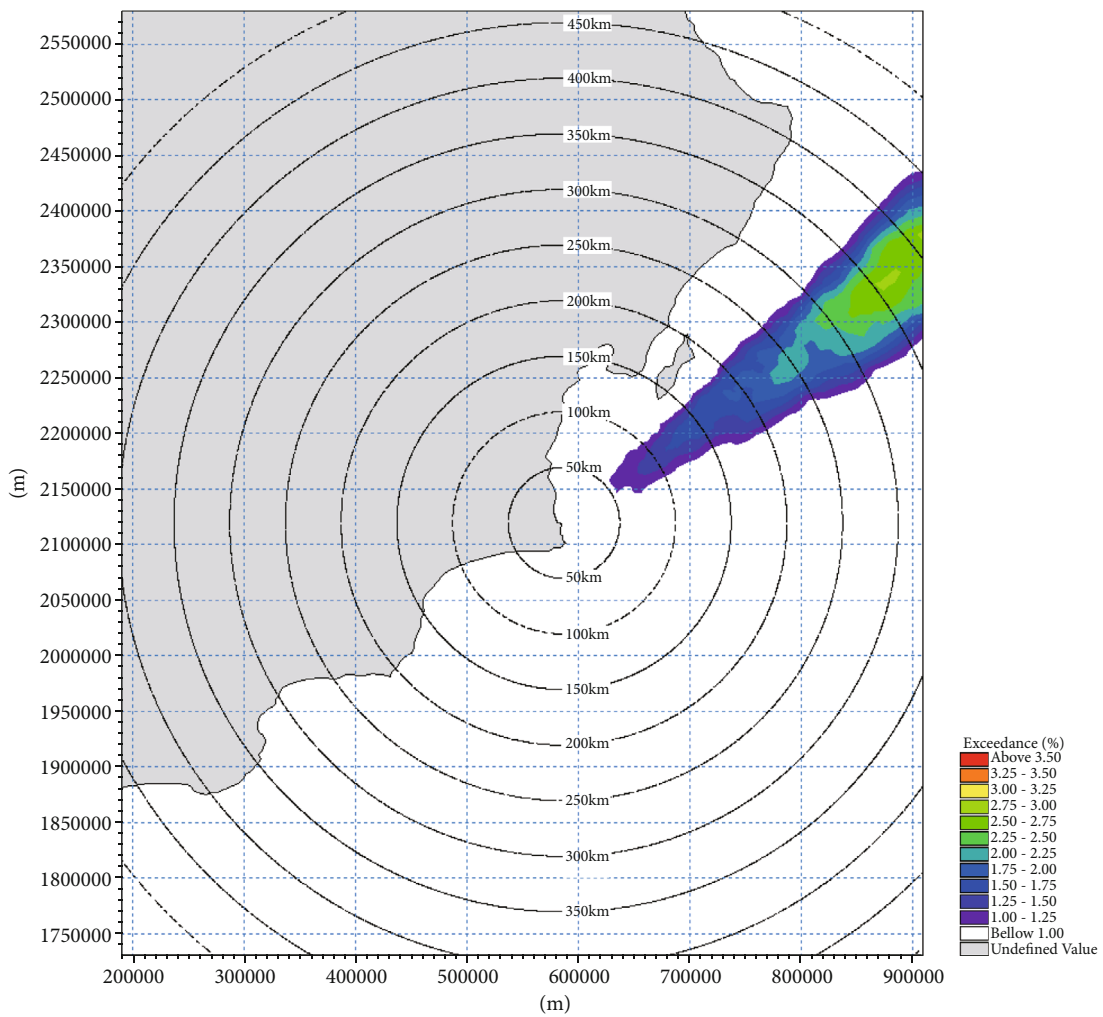


FIGURE 16: Exceedance probability of water surface oil thickness >10 μm for scenario 1 (sub-surface blowout: 16,000 m<sup>3</sup> spill at SPM1)—full model extent.

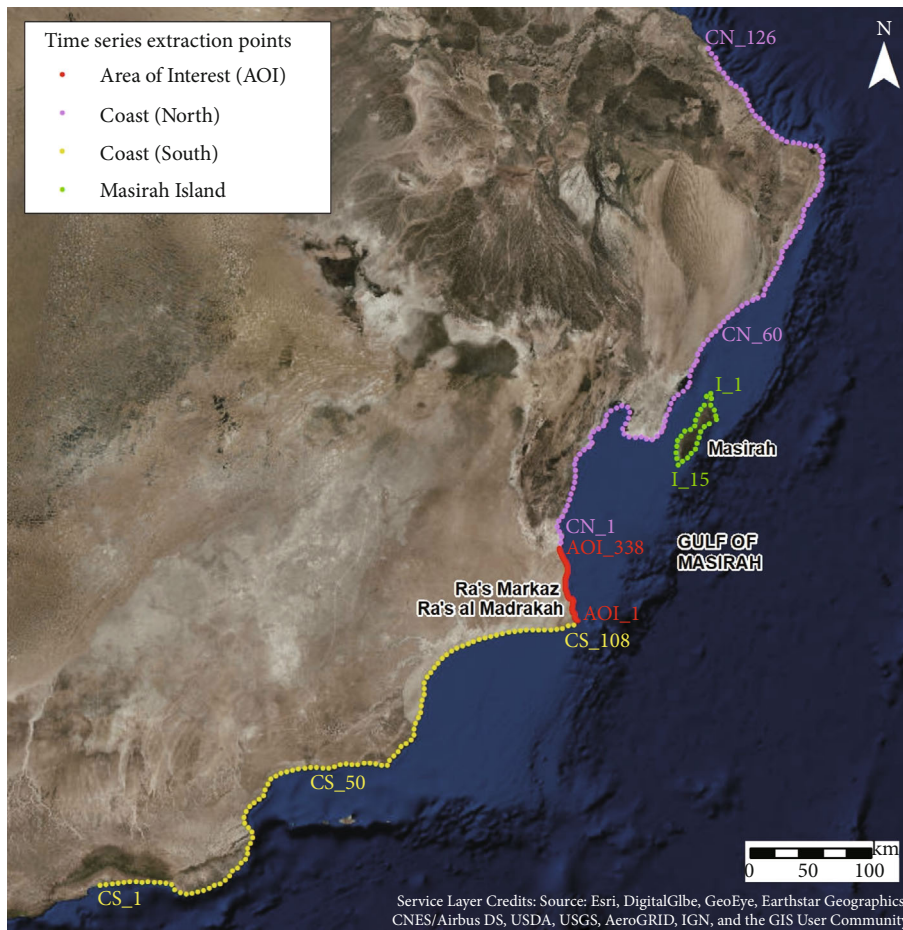


FIGURE 17: Shoreline points that time series data were extracted for duration statistical analysis.

3.6. *Run Scenarios.* The following three spill scenarios were simulated:

- (a) Surface blowout:  $16,000m^3$  oil release within one hour at SPM1
- (b) Subsea blowout;  $16,000m^3$  oil release within one hour at the trench exit of buried oil pipe
- (c) Spill from vessel collision at the mostly likely vessel collision area:  $4,500m^3$  oil release within six hours

The most likely vessel collision area is at San Carlos Banks (shown in Figure 5) which is approximately 26 km in the north of the site. A comparison of historic oil spills (from ITOPF [39]) shows that spills exceeding 700 tonnes (approx.  $700m^3$ ) are rare (and much rarer than oil spills smaller than 700 tonnes) (refer to Figure 11). The oil spill due to grounding of approx. 4,500 tonnes ( $4,500m^3$ ) is therefore considered a reasonable figure based on historical spill data.

The initial oil spill locations are shown in Figure 12. It should be noted that scenarios I and II above also are deemed to cover, in terms of oil release volume and location, the scenario of two VLCCs colliding at the SPM location. From a planning and response perspective, minor variations in the release point are not considered significant. With

regard to oil spills related to hose cleaning, the volumes associated with this type of oil spill is considered minimal, and it is not deemed required to model such a scenario.

#### 4. Model Results and Discussion

4.1. *Map of Maximum Oil Concentration.* Results were extracted over the entire model domain to investigate the extent of the oil spill plumes. Figures 13 and 14 provide two dimensional maps of maximum oil concentration (of 60-day simulation) for the oil spill scenario 1 under typical summer and winter wind conditions. Maps of maximum oil concentration were selected from oil release at 13 different tidal phases and neap and spring tidal cycles for the worst cases (i.e., maximum extent of oil spreading). It should be noted that concentrations of dissolved aromatics in the water column are usually small and not considered in the oil spill response plan and have therefore not been considered.

4.2. *Temporal Changes in Oil Concentration at Initial Spill Locations.* The model results were extracted at the initial spill locations (shown in Figure 15) to investigate the changes in oil concentration at those locations. Figure 15 illustrates a sample time-series plot of oil concentration at SPM1 for oil spill scenario 1 under typical winter wind

condition. It is noted that oil concentration raised immediately after oil spill, but oil concentration is reduced to ambient level within 1-2 days. This is because oil movement under prevailing winds is almost in a transverse direction to the tidal flow. As a result, spill oil does not return to its release point under the influence of prevailing winds.

**4.3. Probability of Oil Contamination.** The probabilities of water surface oiling have been processed from model simulations for annual wind frequency for oil thickness above  $0.01\ \mu\text{m}$ ,  $1\ \mu\text{m}$ , and  $10\ \mu\text{m}$  and also for oil concentration above 58 ppb. The contour maps of probabilities of thickness above  $0.01\ \mu\text{m}$ ,  $1\ \mu\text{m}$ , and  $10\ \mu\text{m}$  and of oil concentration above 58 ppb are identical. The reason is that the accuracy of this oil spill model was limited to oil thickness above  $10\ \mu\text{m}$ . Figure 16 shows a two-dimensional map of probabilities of oil thickness above  $10\ \mu\text{m}$  for the oil spill scenario 1.

**4.4. Shoreline Impact.** In order to analyze shoreline impact by oil spill, time series of oil concentration and thickness were extracted from model results. Those shoreline points are illustrated in Figure 17. Points in the “Area of Interest” (AOI) are set to 200 m interval between Ras Madrakah and South of Duqm. Points in other coastlines, namely “Coast North” (CN series), “Coast South” (CS series) and “Island” (I series), are set at 5 km interval. The impact to “Coast North” is limited to the Gulf of Masirah. “Coast South” received little oil except those points close to Ras Madrakah headland.

## 5. Conclusive Remarks

The modelling results indicate that both tidal currents and wind drag force have a significant effect in oil spill movement. The dominant wind in the area is South-westerly wind during the summer monsoon and North-easterly wind during the winter monsoon, but South-westerly wind is far stronger and last longer than the North-easterly wind. As a result, oil spill trajectory is most likely towards offshore to North-east during the summer period (April to September). During the winter period (November–January), oil spill would move towards shore under North-westerly winds. Once oil reaches shore, it would stay at shore permanently and eventually sink to seabed or beach in the simulation. Although the model does not consider longshore drift by waves, oil movement along shore by waves would be a slow process. Therefore, the impact of oil spill during the winter monsoon would be limited to local area around Ras Markaz. Oil can spread quickly to offshore under South-westerly wind, and oil can reach to as far as Masirah Island in the north. However, oil concentrations at the key environmentally sensitive locations are low except Coral Head 1. It is noticed that oil movement under prevailing winds is almost in a transverse direction to the tidal flow. As a result, spill oil does not return to its release point under the influence of prevailing winds.

## Data Availability

The datasets used and/or analyzed during the current study are available from the corresponding author on reasonable request.

## Conflicts of Interest

The author declared no potential conflicts of interest with respect to the research, authorship, and/or publication of this paper.

## References

- [1] *Shell DEP 37.91.10.10-Gen, Single Point Mooring System*, 2011.
- [2] R. Maari, *Single Point Mooring*, Principality of Monaco, 1985.
- [3] J. J. Cheng and C. J. Wang, “Crude oil dock development in China: spatial distribution, capacity and problems,” *China Transportation Review*, vol. 39, no. 4, pp. 22–27, 2017.
- [4] Y. Lv, X. Z. Ju, X. F. Li, G. Li, B. H. Dong, and C. T. Zhong, “Study on construction conditions & site selection of catenary anchor leg mooring (CALM) for offshore oil terminal,” *Ocean Engineering Equipment and Technology*, vol. 5, no. 5, pp. 300–304, 2018.
- [5] S. Ryu, A. S. Duggal, C. N. Heyl, and Y. Liu, “Prediction of deepwater oil offloading buoy response and experimental validation,” *International Journal of Offshore and Polar Engineering*, vol. 16, no. 4, pp. 290–296, 2006.
- [6] H. D. Hollister and J. J. Spokes, “The Agbami project: a world class deepwater development,” in *Offshore Technology Conference*, Houston, 2004.
- [7] Y. F. Wang, D. G. Wang, Y. T. Kang, and H. Jin, “Study on oil spill risk management and prevention for single-point mooring systems,” *Ocean Engineering Equipment and Technology*, vol. 1, no. 3, pp. 200–206, 2014.
- [8] W. Guo, Y. X. Wang, M. Xie, and Y. J. Cui, “Modeling oil spill trajectory in coastal waters based on fractional Brownian motion,” *Marine pollution bulletin*, vol. 58, no. 9, pp. 1339–1346, 2009.
- [9] A. H. Al-Rabeh, H. M. Cekirge, and N. Gunay, “A stochastic simulation model of oil spill fate and transport,” *Applied Mathematical Modelling*, vol. 13, no. 6, pp. 322–329, 1989.
- [10] Z. Liu, Q. Chen, Y. Zhang, C. Zheng, B. Cai, and Y. Liu, “Research on transport and weathering of oil spills in Jiaozhou Bight, China,” *Regional Studies in Marine Science*, vol. 51, article 102197, 2022.
- [11] J. A. Fay, “Physical processes in the spread of oil on a water surface,” in *International Oil Spill Conference Proceedings* no. 1, pp. 463–467, Washington, D. C., 1971.
- [12] W. J. Lehr, R. J. Fraga, M. S. Belen, and H. M. Cekirge, “A new technique to estimate initial spill size using a modified fay-type spreading formula,” *Marine Pollution Bulletin*, vol. 15, no. 9, pp. 326–329, 1984.
- [13] A. J. Elliott, “EUROSPILL: oceanographic processes and NW European shelf databases,” *Marine Pollution Bulletin*, vol. 22, no. 11, pp. 548–553, 1991.
- [14] X. B. Chao, N. J. Shankar, and H. F. Cheong, “Two- and three-dimensional oil spill model for coastal waters,” *Ocean Engineering*, vol. 28, no. 12, pp. 1557–1573, 2001.
- [15] S. D. Wang, Y. M. Shen, and Y. H. Zheng, “Two-dimensional numerical simulation for transport and fate of oil spills in seas,” *Ocean Engineering*, vol. 32, no. 13, pp. 1556–1571, 2005.
- [16] P. Sebastiao and C. G. Soares, “Modeling the fate of oil spills at sea,” *Spill Science and Technology Bulletin*, vol. 2, no. 2–3, pp. 121–131, 1995.
- [17] P. Vethamony, K. Sudheesh, M. T. Babu et al., “Trajectory of an oil spill off Goa, eastern Arabian Sea: field observations



- and simulations,” *Environmental pollution*, vol. 148, pp. 438–444, 2007.
- [18] B. Díaz, A. Pavón, and M. Gómez-Gesteira, “Use of a probabilistic particle tracking model to simulate the prestige oil spill,” *Journal of Marine Systems*, vol. 72, no. 1–4, pp. 159–166, 2008.
- [19] W. J. Guo and Y. X. Wang, “A numerical oil spill model based on a hybrid method,” *Marine Pollution Bulletin*, vol. 58, no. 5, pp. 726–734, 2009.
- [20] A. J. Mariano, V. H. Kourafalou, A. Srinivasan et al., “On the modeling of the 2010 gulf of Mexico oil spill,” *Dynamics of Atmospheres and Oceans*, vol. 52, no. 1–2, pp. 322–340, 2011.
- [21] F. Yu, J. Li, S. Cui, Y. Zhao, Q. Feng, and C. Ge, “A hindcast method to simulate oil spill trajectories for the Bohai Sea, Northeast China,” *Ocean Engineering*, vol. 124, pp. 363–370, 2016.
- [22] R. Perianez, “A Lagrangian oil spill transport model for the Red Sea,” *Ocean Engineering*, vol. 217, article 107953, 2020.
- [23] S. Naz, M. F. Iqbal, I. Mahmood, and M. Allam, “Marine oil spill detection using synthetic aperture radar over Indian ocean,” *Marine Pollution Bulletin*, vol. 162, article 111921, 2021.
- [24] M. Y. Omar, M. F. Shehada, A. K. Mehanna, A. H. Elbatran, and M. M. Elmesiry, “A case study of the Suez Gulf: modelling of the oil spill behavior in the marine environment,” *Egyptian Journal of Aquatic Research*, vol. 47, no. 4, pp. 345–356, 2021.
- [25] D. Simecek-Beatty and W. J. Lehr, “Oil spill forecast assessment using fractions skill score,” *Marine Pollution Bulletin*, vol. 164, article 112041, 2021.
- [26] Q. Pan, X. Zhu, L. Wan et al., “Operational forecasting for Sanchi oil spill,” *Applied Ocean Research*, vol. 108, article 102548, 2021.
- [27] P. Sebastiao and C. G. Soares, “Uncertainty in predictions of oil spill trajectories in a coastal zone,” *Journal of Marine Systems*, vol. 63, no. 3–4, pp. 257–269, 2006.
- [28] A. Azevedo, A. Oliveira, A. B. Fortunato, J. Zhang, and A. M. Baptista, “A cross-scale numerical modeling system for management support of oil spill accidents,” *Marine Pollution Bulletin*, vol. 80, no. 1–2, pp. 132–147, 2014.
- [29] A. K. Mishra and G. S. Kumar, “Weathering of oil spill: modeling and analysis,” *Aquatic Procedia*, vol. 4, pp. 435–442, 2015.
- [30] M. L. Spaulding, “State of the art review and future directions in oil spill modeling,” *Marine Pollution Bulletin*, vol. 115, no. 1–2, pp. 7–19, 2017.
- [31] J. M. Price, W. R. Johnson, C. F. Marshall, Z. G. Ji, and G. B. Rainey, “Overview of the oil spill risk analysis (OSRA) model for environmental impact assessment,” *Spill Science and Technology Bulletin*, vol. 8, no. 5–6, pp. 529–533, 2003.
- [32] A. Berry, T. Dabrowski, and K. Lyons, “The oil spill model OILTRANS and its application to the Celtic Sea,” *Marine Pollution Bulletin*, vol. 64, no. 11, pp. 2489–2501, 2012.
- [33] A. C. Toz and M. Buber, “Performance evaluation of oil spill software systems in early fate and trajectory of oil spill: comparison analysis of OILMAP and PISCES 2 in Mersin bay spill,” *Environmental Monitoring and Assessment*, vol. 190, no. 9, p. 551, 2018.
- [34] T. Nordam, C. J. Beegle-Krause, J. Skancke, N. Raymond, and M. Reed, “Improving oil spill trajectory modelling in the arctic,” *Marine Pollution Bulletin*, vol. 140, pp. 65–74, 2019.
- [35] K. Kampouris, V. Vervatis, J. Karagiorgos, and S. Sofianos, “Oil spill model uncertainty quantification using an atmospheric ensemble,” *Ocean Science*, vol. 17, no. 4, pp. 919–934, 2021.
- [36] Y. Z. Chen, “Development of an oil spill model adaptable to exposure and submergence conversion of tidal flats: a case study in the Changjiang Estuary,” *Marine Pollution Bulletin*, vol. 171, article 112715, 2021.
- [37] A.-L. Balogun, S. Yekeen, B. Pradhan, and K. Yusof, “Oil spill trajectory modelling and environmental vulnerability mapping using GNOME model and GIS,” *Environmental Pollution*, vol. 268, no. Part A, article 115812, 2021.
- [38] L. Lopez and S. L. Monaco-Trupiano, “Comparison of crude oil source-related indicators based on C15-, C15+ and C40+ parameters,” *Journal of Oil, Gas, and Alternative Energy Sources*, vol. 6, no. 3, pp. 53–70, 2016.
- [39] *ITOPF Handbook*, 2021, [https://www.itopf.org/fileadmin/data/Documents/Company\\_Lit/Oil\\_Spill\\_Stats\\_2019.pdf](https://www.itopf.org/fileadmin/data/Documents/Company_Lit/Oil_Spill_Stats_2019.pdf).